JOURNAL OF APPLIED ELECTROCHEMISTRY 25 (1995) 1023–1030

A wall-jet electrode reactor and its application to the study of electrode reaction mechanisms
Part II: A general computational method for the mass transport problems involved

P. LAEVERS, A. HUBIN, H. TERRYN, J. VEREECKEN

Department of Metallurgy, Electrochemistry and Materials Science, Vrije Universiteit Brussel, Pleinlaan 2, 1050 Brussels, Belgium

Received 30 January 1995; Revised 28 February 1995

A numerical computational method to solve the problems of mass transport to the impinged surface of a wall-jet electrode reactor is put forward, thus providing the necessary tool for a quantitative electrochemical investigation of the mechanism of electrode processes, using a wall-jet electrode reactor as a hydrodynamic electrode system. The computational method is based on a second order-correct implicit finite difference approach and a coordinate transformation making a simple Cartesian space discretization compatible with efficient computing, thus allowing the computations to be performed on a personal computer. The computational approach is demonstrated through calculation of a single step chronoamperometric transient for a simple one electron transfer reaction and shown to be accurate by comparing the computed with experimentally determined current transients using as a model reaction the reduction of ferricyanide ions at a platinum electrode surface from a 0.01 M $K_3Fe(CN)_6$–0.01 M $K_4Fe(CN)_6$ solution containing 1 M KCl as supporting electrolyte

List of symbols

- a nozzle diameter (m)
- C_i concentration of electroactive species i (mol m^{-3})
- $\underline{C_i}$ normalized concentration of electroactive species i
- D_i diffusion coefficient of the electroactive species i (m^2 s^{-1})
- E electrode potential (V vs SCE)
- E_0 equilibrium potential (V vs SCE)
- F Faraday's constant (C mol^{-1})
- η dimensionless parameter, describing the distance normal to the impinged electrode
- H distance between the working electrode and the tip of the nozzle (m)
- I electrode current (A)
- k_r constant linking the typical velocity of the wall-jet to the mean velocity in the nozzle
- M flux of exterior momentum flux
- ν kinematic viscosity (m^2 s^{-1})
- r distance along the impinged electrode in cylindrical pole coordinates having their origin at the intersection of the jet axis and the electrode surface
- R radius of the impinged electrode (m)
- τ dimensionless time
- t time (s)
- v_r velocity component along the impinged electrode (m s^{-1})
- v_z velocity component normal to the impinged electrode (m s^{-1})
- V_f volume flow rate (m^{-3} s^{-1})
- ξ dimensionless parameter, describing the distance normal to the impinged electrode
- z distance normal to the impinged electrode in cylindrical pole coordinates having their origin at the intersection of the jet axis and the electrode surface (m)

1. Introduction

In a previous paper [1] the design and construction of a reactor exhibiting true wall-jet electrode hydrodynamics was reported. The reactor is characterized by the size of the impinged electrode surface and is designed to suit the need for a large working electrode surface area in the study of the mechanism of the a.c. electrolytic graining of rolled aluminium substrates. In this paper, a numerical computation method is put forward, to solve the mass transport problems involved in using the wall-jet electrode reactor as a hydrodynamic electrode system in a quantitative electrochemical investigation of electrode reaction mechanisms. The computational method developed, is based on a second order correct-implicit finite difference approach and a space coordinate transformation making the use of a simple Cartesian grid compatible with efficient computing, thus allowing the calculations to be performed on a personal computer. The

0021-891X

computational method hereby particularly distinguishes itself from the one hitherto published [2–5], being based on a mainly first order-correct implicit finite difference approach and a space discretization according to a grid expanding in size, in proportion to the concentration boundary layer thickness across the impinged surface of a wall-jet electrode reactor.

Since potential step chronoamperometry is a powerful tool in the mechanistic study of electrode processes, the general computational method is demonstrated through the computation of a single step chronoamperometric transient for a simple one electron transfer reaction. Current transients recorded in the newly designed reactor are reported, confirming the validity of the computational method.

2. Basic equations

The mathematical formulation of mass transport to the impinged surface of a wall-jet electrode reactor and more in particular its level of approximation, has major consequences, not only for the validity and accuracy of the computational method, but also for the computational strategy itself, since the mathematical formulation is the first step in such a strategy. Therefore, in this paragraph, the mathematical formulation is elaborated, pointing out all approximations made; the numerical computational method itself is presented and evaluated in the subsequent paragraphs.

Mass transport of an electroactive species i, of minor concentration C_i (mol m^{-3}) in a solution containing an excess of indifferent supporting electrolyte, to the impinged surface of a wall-jet electrode reactor is described by [6, 7]

$$\frac{\partial C_i}{\partial t} = D_i \frac{\partial^2 C_i}{\partial z^2} - v_r \frac{\partial C_i}{\partial r} - v_z \frac{\partial C_i}{\partial z} \tag{1}$$

where r and z are the distances along and normal to the impinged electrode in cylindrical pole coordinates having their origin at the intersection of the jet axis and the electrode surface, v_r and v_z the corresponding velocity components and where D_i (m^2 s^{-1}) is the diffusion coefficient of the electroactive species. In writing the above equation, commonly known as the convective diffusion equation, it is assumed that homogeneous reactions producing or consuming i do not occur. The radial diffusion has been omitted, which can be understood from the following observation. Radial diffusion effects can only become important in regions where the solution is most stagnant, that is, near the outer radius of the impinged electrode surface [1]. However, in this region, the radial concentration gradients are necessarily small [3, 4] and thus the effect of radial diffusion upon the concentration changes in the wall-jet can be neglected [8, 9].

It is the integration of Equation 1, with the appropriate boundary conditions, which yields the quantities of interest, being the time dependent concentration profile of the electroactive species and derived from it, the electrode current. To perform the integration, the velocity components v_r and v_z, determined by the fluid dynamics, must be known.

The fluid dynamics are governed by the continuity and Navier–Stokes equation, which, following the Prandtl boundary layer theory [10], reduce to

$$\frac{\partial v_r}{\partial r} + \frac{\partial v_z}{\partial z} = 0 \tag{2}$$

and

$$v_r \frac{\partial v_r}{\partial r} + v_z \frac{\partial v_r}{\partial z} = \nu \frac{\partial^2 v_r}{\partial z^2} \tag{3}$$

for a wall-jet at hydrodynamic equilibrium, respectively. This problem was studied by Glauert [11], who found that an exact similarity solution of the above boundary layer equations can be obtained, if

$$v_r = v_z = 0 \quad \text{at } z = 0 \tag{4}$$

and

$$v_r \longrightarrow 0 \quad \text{as } z \longrightarrow \infty \tag{5}$$

are used as boundary conditions. The solution is thus strictly valid only for a fluid jet of zero width, submerged in a stationary medium of that fluid, which impinges perpendicularly onto a plane wall and spreads out radially over it. Though, it can be used as a good approximation of the velocity distribution in a wall-jet electrode reactor, provided that the width of the jet is small compared to the size of the impinged electrode and the reactor walls do not interfere with the flow across the impinged surface [8, 9, 12].

Following Glauert [11], the velocity distribution is expressed in terms of a dimensionless parameter η describing the distance normal to the impinged electrode

$$\eta = \left(\frac{135M}{32\nu^3 r^5}\right)^{1/4} z \tag{6}$$

where ν (m^2 s^{-1}) is the kinematic viscosity of the fluid and M is the flux of exterior momentum flux, defined by

$$M = \int_0^\infty r v_r \left(\int_0^\infty r v_r^2 \mathrm{d}r \right) \mathrm{d}r \tag{7}$$

As proved by Glauert [11], M is constant throughout the wall-jet and can be approximated by

$$M = \tfrac{1}{2}(\text{typical wall-jet velocity}) \left(\frac{\text{volume flow rate}}{\text{radial}} \right)^2 \tag{8}$$

If the typical wall-jet velocity is assumed to be proportional to the mean velocity in the jet at the nozzle exit, Equation 8 becomes

$$M = \frac{1}{2} k_r' \left(\frac{4V_f}{\pi a^2}\right) \left(\frac{V_f}{2\pi}\right)^2 = \frac{k_r'^4 V_f^3}{2\pi^3 a^2} \tag{9}$$

where V_f (m^3 s^{-1}) is the volume flow rate, a (m) is the nozzle diameter and k_r' is the proportional factor, to be determined by experiment for the reactor used [12].

The radial and axial velocity components are given

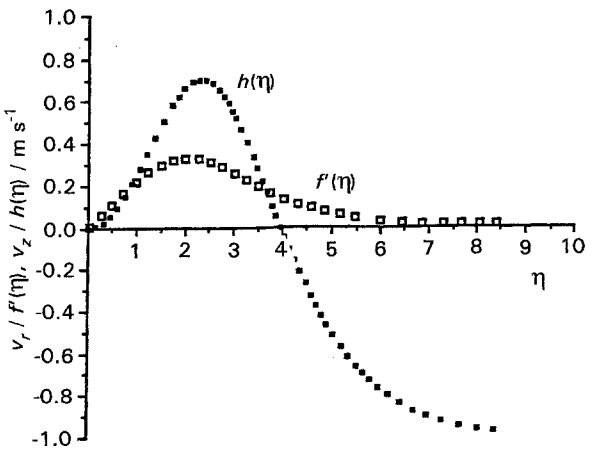

Fig. 1. Variation of the radial and axial velocity with η, illustrated by plotting the functions $f'(\eta)$ and $h(\eta)$, respectively.

by

$$v_r = \left(\frac{15M}{2\nu r^3}\right)^{1/2} f'(\eta) \tag{10}$$

$$v_z = \frac{3}{4}\left(\frac{40M\nu}{3r^5}\right)^{1/4} h(\eta) \tag{11}$$

where

$$f'(\eta) = \tfrac{2}{3}g(1-g^3) \tag{12}$$

$$f(\eta) = g^2 \tag{13}$$

$$h(\eta) = \tfrac{5}{3}\eta f'(\eta) - f(\eta) \tag{14}$$

and

$$\eta = \ln\left(\frac{(1+g+g^2)^{1/2}}{1-g}\right) + \sqrt{3}\tan^{-1}\left(\frac{\sqrt{3}g}{2+g}\right) \tag{15}$$

with η varying between 0 and ∞ as g goes from 0 to 1 [8, 11].

From Equations 10 and 11 it is clear that both the radial and axial velocity components decrease with increasing r. The variation of v_r and v_z with η is illustrated in Fig. 1, by plotting the functions $f'(\eta)$ and $h(\eta)$, respectively. From these plots it can be seen that the radial and axial velocity components are zero at the impringed surface, as dictated by the boundary conditions. Starting from zero, the radial velocity component increases, reaching a maximum at $\eta = 2.01$ and then declines back to zero. The axial velocity component increases from zero, at first with a parabolic dependence, passes through a maximum at $\eta = 2.31$ and drops back to zero for $\eta = 3.96$. For these values of η, the flow is away from the electrode. For values of η larger than 3.96, $h(\eta)$ is negative, reaching a limit value of -1. In this region the flow is thus towards the electrode. In evidence, a boundary exists at $\eta = 3.96$ which separates the flow towards and away from the electrode, meaning that the impinged surface is in contact only with fluid which just passed through the nozzle [8,9]. The boundary and the schematic stream lines are shown in Fig. 2.

Since concentration changes occur in a fluid layer adjacent to the impinged electrode, of which the

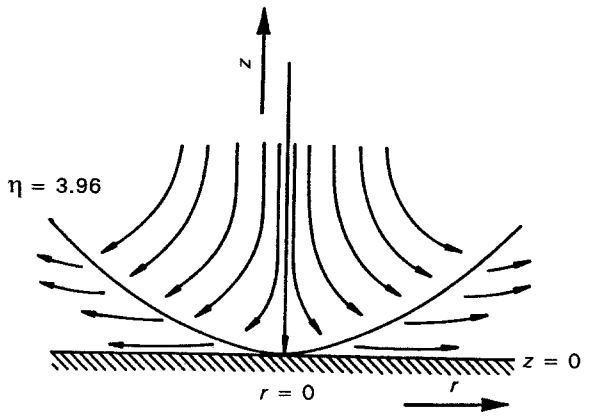

Fig. 2. Schematic illustration of the pattern of flow in the vicinity of the impinged surface [8].

thickness is in proportion of $(D_i/\nu)^{1/3}$ to the hydrodynamic boundary layer thickness [7, 13,14] and typical values of D_i and ν for most electrolytes are 10^{-9} m^2 s^{-1} and 10^{-6} m^2 s^{-1}, respectively, the velocity distribution of particular interest is that for $0 < \eta < \eta_c$ with $\eta_c \cong 3.96(D_i/\nu)^{1/3} < 1$. For these small values of η Equation 15 can be approximated by

$$g \cong \tfrac{1}{3}\eta \tag{16}$$

so that, taking into account Equations 12 to 14 and Equation 6, the equations for the radial (Equation 10) and axial (Equation 11) velocity component reduce to [8]

$$v_r = \left(\frac{125M^3}{216\nu^5}\right)^{1/4} r^{-11/4} \tag{17}$$

and

$$v_z = \frac{7}{8}\left(\frac{125M^3}{216\nu^5}\right)^{1/4} z^2 r^{-15/4} \tag{18}$$

These approximated expressions for v_r and v_z can thus, in most circumstances, be used instead of the full expressions, when integrating the convective diffusion equation.

3. Experimental

The single step chronoamperometric transient measurements to test the validity of the computational method presented, were carried out for the reduction of ferricyanide ions at a platinum electrode surface from a 0.01 M $K_3Fe(CN)_6$–0.01 M $K_4Fe(CN)_6$ solution containing 1 M KCl as supporting electrolyte. The electrode potential was stepped from its equilibrium potential ($E_0 = 2.28 \times 10^{-1}$ V vs SCE) to a potential for which mass transport is rate determining (between -4.50×10^{-1} and -5.00×10^{-1} V vs SCE, depending on the reactor parameters used [1]), since, for large overpotentials, the electrode reaction mechanism for the reduction of ferricyanide ions at a platinum electrode surface is known to be well modelled by a simple one electron transfer reaction [4]. The experimental details were reported in a previous paper [1], concerning the design and construction of the wall-jet electrode reactor used.

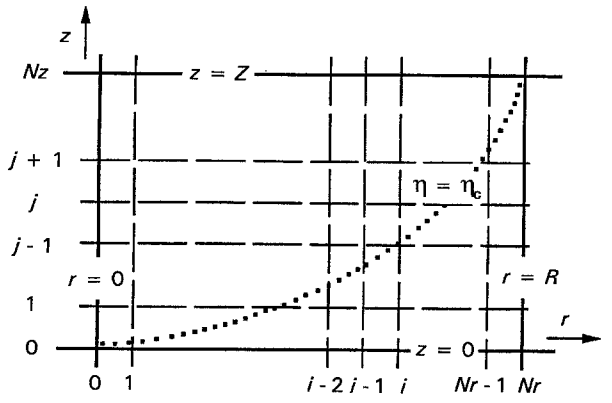

Fig. 3. The obvious discretization of the physical (r,z)-plane. $r = i\Delta r$ with $\Delta r = R/Nr$ for $i = 0, 1, \ldots, Nr$; $z = j\Delta z$ with $\Delta z = Z/Nr$ for $j = 0, 1, \ldots, n_z$.

4. Results and discussion

4.1. *Computation of a chronoamperometric transient*

Consider a simple one electron transfer reaction

$$A + e^- \longleftrightarrow B \tag{19}$$

at the impinged surface of a wall-jet electrode reactor, in a solution containing an excess of indifferent supporting electrolyte, with the electrode potential being stepped from its equilibrium potential to a potential at which the kinetics for the reduction of A become so rapid that mass transport of the electroactive species A to the impinged surface is controlling the rate of reaction.

4.1.1. Mathematical model. The convective diffusion equation and boundary conditions relevant to the defined problem can be formulated as

$$\frac{\partial \underline{C}_A}{\partial t} = D_A \frac{\partial^2 \underline{C}}{\partial z^2} - br^{-11/4}\frac{\partial \underline{C}_A}{\partial r} - \frac{7}{8}bz^2 r^{-15/4}\frac{\partial \underline{C}_A}{\partial z} \tag{20}$$

$$t \leqslant 0 \quad 0 \leqslant r \leqslant R \quad 0 \leqslant z \tag{21}$$

$$\underline{C}_A = 1$$

$$t > 0 \quad 0 \leqslant r \leqslant R \quad z = 0 \tag{22}$$

$$\underline{C}_A = 0$$

$$0 \leqslant r \leqslant R \quad z \longrightarrow \infty \tag{23}$$

$$\underline{C}_A = 1$$

$$r = 0 \quad 0 < z \tag{24}$$

$$\underline{C}_A = 1 \tag{24a}$$

$$\frac{\partial \underline{C}_A}{\partial r} = 0 \tag{24b}$$

where

$$\underline{C}_A = C_A / C_A^{\text{bulk}} \tag{25}$$

is the normalized concentration of A,

$$b = \left(\frac{125M^3}{216\nu^5}\right)^{1/4} \tag{26}$$

and R is the radius of the impinged electrode.

Equation 22 expresses that, under mass transport–limited conditions, the electroactive species A can not coexist with the electrode; the surface concentration of A must therefore equal zero. The boundary conditions at $r = 0$, Equations 24(a) and 24(b), express that the fluid passing through the nozzle and the stationary surrounding fluid are of equal composition and that in the centre of the jet the radial flux of A is zero, respectively. Since the concentration boundary layer is infinitesimally thin at $r = 0$, the above conditions apply for all $z > 0$.

4.1.2. Numerical scheme. The above partial differential equation, with the appropriate boundary conditions, is solved using the alternating direction implicit finite difference method. It is the discernment of the boundary conditions at $r = 0$ and in particular of the boundary condition expressed by Equation 24(b), together with the use of an upwind scheme in the radial direction (discussed below), which allows this second order-correct finite difference method to be employed.

Space discretization

The finite difference method requires a spatial grid with a high degree of regularity. In particular, it requires the grid to be set up so that, in a two-dimensional space, the grid points are located at the intersections of two families of rectilinear lines [15, 16].

The obvious discretization of the (r,z)-plane, shown in Fig. 3, is likely to be unsatisfactory, given the highly nonuniform accessibility of the electrode. In evidence, if the mesh size is chosen sufficiently small to cover the thin end of the concentration boundary layer with a number of grid points large enough to ensure convergence, the total number of grid points will be inconveniently large, since the same mesh size is applied at the edge of the electrode where the concentration boundary layer is much thicker. Furthermore, for small values of r the greater part of the grid points lies outside the concentration boundary layer, where $\underline{C}_A$ is known.

These difficulties are overcome if the space discretization, shown in Fig. 4, is performed after transformation of the physical (r,z)-plane in the dimensionless computational (ξ,η)-plane, using

$$\eta = \left(\frac{135M}{32\nu^3 r^5}\right)^{1/4} z \tag{6}$$

and

$$\xi = r/R \tag{27}$$

as coordinate transformation formulas. As can be seen from comparison of Figs 3 and 4, the use of a simple Cartesian grid in the computational plane comes down to using an expanding grid restricted to the concentration boundary layer in the (r,z)-plane. Thus, the coordinate transformation makes the use of a simple Cartesian space discretization scheme compatible with efficient computation.

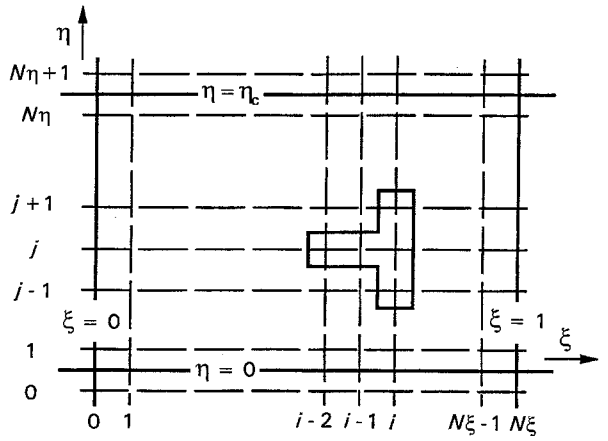

Fig. 4. The grid used to discretize the computational (ξ, η)-plane. $\xi = i\Delta\xi$ with $\Delta\xi = 1/N\xi$ for $i = 0, 1, \ldots, N\xi$; $\eta = (j - 1/2)\Delta\eta$ with $\Delta\eta = \eta_c/N\eta$ for $i = 0, 1, \ldots, N\eta + 1$.

Notice that the grid points in Fig. 4 are shifted one-half an increment from the boundary $\eta = 0$, thus avoiding having to specify the value of $\underline{C}_A$ at the impingement point $\xi = \eta = 0$.

Equation discretization

In the computational (ξ, η)-plane, Equation 20 reduces to

$$\xi^{5/2}\frac{\partial \underline{C}_A}{\partial \tau} = \frac{\partial^2 \underline{C}_A}{\partial \eta^2} - \frac{8\nu}{27D_A}\xi\eta\frac{\partial \underline{C}_A}{\partial \xi} + \frac{\nu}{9D_A}\eta^2\frac{\partial \underline{C}_A}{\partial \eta} \tag{28}$$

where τ is the dimensionless time, defined as

$$\tau = \left(\frac{135M}{32\nu^3R^5}\right)^{1/2} D_A t \tag{29}$$

The appropriate boundary conditions are

$$\tau \leqslant 0 \qquad 0 \leqslant \xi \leqslant 1 \qquad 0 \leqslant \eta \leqslant \eta_c \tag{30}$$

$$\underline{C}_A = 1$$

$$\tau > 0 \qquad 0 \leqslant \xi \leqslant 1 \qquad \eta = 0 \tag{31}$$

$$\underline{C}_A = 0$$

$$0 \leqslant \xi \leqslant 1 \qquad \eta = \eta_c \tag{32}$$

$$\underline{C}_A = 1$$

$$\xi = 0 \qquad 0 < \eta \leqslant \eta_c \tag{33}$$

$$\underline{C}_A = 1 \tag{33a}$$

$$\frac{\partial \underline{C}_A}{\partial \xi} = 0 \tag{33b}$$

For the discretization of Equation 28 the alternating direction implicit method is used [15–18]. This method involves the alternated use of two finite difference equivalents to Equation 28. For the first finite difference equation the equivalents to the η-derivatives are written at the new time level $\tau_{n+1/2}$, using second order correct central finite difference approximations. The finite difference equivalent to $\partial \underline{C}_A/\partial \xi$ is written at the old time level τ_n. Given the centrifugal character of the flow in a wall-jet electrode reactor and the predominance of the radial convection over the radial

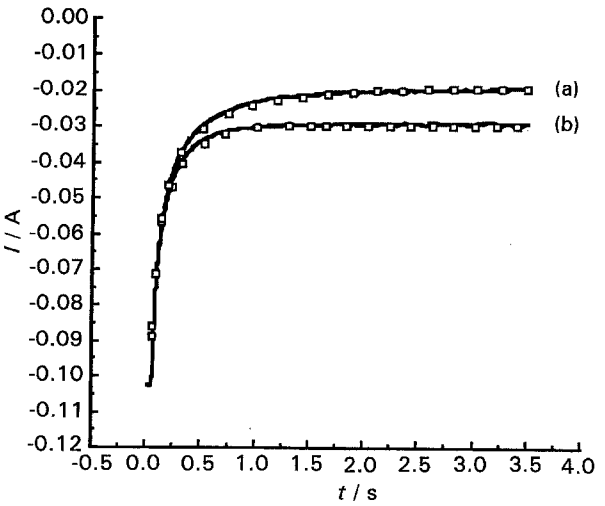

Fig. 5. Illustration of the agreement between computed and experimentally determined chronoamperometric transients using as a model reaction the reduction of ferricyanide ions at a platinum electrode surface from a 0.01 M $K_3Fe(CN)_6$–0.01 M $K_4Fe(CN)_6$ solution containing 1 M KCl as supporting electrolyte ($E_0 = 2.28 \times 10^{-1}$ V vs SCE, $E = -4.50 \times 10^{-1}$ V vs SCE for (a) and -4.70×10^{-1} V vs SCE for (b), $R = 2.000 \times 10^{-2}$ m, $a = 2.00 \times 10^{-3}$ m, $H/a = 13$, $k_r = 0.82$, $D_A = 7.3\,m^2\,s^{-1}$). (a) $V_f = 1.689 \times 10^{-6}\,m^3\,s^{-1}$; (b) $V_f = 2.981 \times 10^{-6}\,m^3\,s^{-1}$.

diffusion, the ξ-derivative is approximated by the second order correct backward finite difference equivalent. The resulting finite difference equation is

$$\begin{aligned}
&(i\Delta\xi)^{5/2}\frac{\underline{C}_A^{i,j,n+1/2} - \underline{C}_A^{i,j,n}}{(\Delta\tau/2)} \\
&= \frac{\underline{C}_A^{i,j-1,n+1/2} - 2\underline{C}_A^{i,j,n+1/2} + \underline{C}_A^{i,j+1,n+1/2}}{(\Delta\eta)^2} \\
&\quad - \frac{8\nu}{27D_A}(i,\Delta\xi)((j-1/2)\Delta\eta) \\
&\quad \times \frac{\underline{C}_A^{i-2,j,n} - 4\underline{C}_A^{i-1,j,n} + 3\underline{C}_A^{i,j,n}}{2\Delta\xi} \\
&\quad + \frac{\nu}{9D_A}((j-1/2)\Delta\eta)^2\frac{\underline{C}_A^{i,j+1,n+1/2} - \underline{C}_A^{i,j-1,n+1/2}}{2\Delta\eta}
\end{aligned} \tag{34}$$

which can be rearranged to

$$\begin{aligned}
&\left(\frac{\nu}{18D_A}\left(j-\frac{1}{2}\right)^2\Delta\eta - \frac{1}{(\Delta\eta)^2}\right)\underline{C}_A^{i,j-1,n+1/2} \\
&\quad + 2\left(\frac{(i\Delta\xi)^{5/2}}{\Delta\tau} + \frac{1}{(\Delta\eta)^2}\right)\underline{C}_A^{i,j,n+1/2} \\
&\quad - \left(\frac{\nu}{18D_A}\left(j-\frac{1}{2}\right)^2\Delta\eta + \frac{1}{(\Delta\eta)^2}\right)\underline{C}_A^{i,j+1,n+1/2} \\
&= -\left(\frac{4\nu}{27D_A}i\left(j-\frac{1}{2}\right)\Delta\eta\right)\underline{C}_A^{i-2,j,n} \\
&\quad + \left(\frac{16\nu}{27D_A}i\left(j-\frac{1}{2}\right)\Delta\eta\right)\underline{C}_A^{i-1,j,n} \\
&\quad + \left(2\frac{(i\Delta\xi)^{5/2}}{\Delta\tau} - \frac{4\nu}{9D_A}i\left(j-\frac{1}{2}\right)\Delta\eta\right)\underline{C}_A^{i,j,n}
\end{aligned} \tag{35}$$

The above equation contains three values of the dependent variable at the unknown time level $\tau_{n+1/2}$, arranged along the vertical part of the T shown in Fig. 4 and three values of $\underline{C}_A$ at the known time level τ_n, arranged along the horizontal part of that T. Consequently, Equation 35 is implicit in the η-direction and explicit in the ξ-direction. Application of the boundary conditions at $\eta = 0$ and $\eta = \eta_c$ to Equation 35 results in

$$\left(\frac{2(i\Delta\xi)^{5/2}}{\Delta\tau} + \frac{3}{(\Delta\eta)^2} - \frac{\nu}{72D_A}\Delta\eta\right)\underline{C}_A^{i,1,n+1/2} - \left(\frac{\nu}{72D_A}\Delta\eta + \frac{1}{(\Delta\eta)^2}\right)\underline{C}_A^{i,2,n+1/2} = -\left(\frac{2\nu}{27D_A}i\Delta\eta\right)\underline{C}_A^{i-2,1,n} + \left(\frac{8\nu}{27D_A}i\Delta\eta\right)\underline{C}_A^{i-1,1,n} + \left(2\frac{(i\Delta\xi)^{5/2}}{\Delta\tau} - \frac{2\nu}{9D_A}i\Delta\eta\right)\underline{C}_A^{i,1,n} \quad (36)$$

for $j = 1$, as $\underline{C}_A^{i,0} = -\underline{C}_A^{i,1}$ at the electrode surface and

$$\left(\frac{\nu}{18D_A}\left(N\eta - \frac{1}{2}\right)^2\Delta\eta - \frac{1}{(\Delta\eta)^2}\right)\underline{C}_A^{i,N\eta-1,n+1/2} + \left(2\frac{(i\Delta\xi)^{5/2}}{\Delta\tau} + \frac{\nu}{18D_A}\left(N\eta - \frac{1}{2}\right)^2\Delta\eta + \frac{3}{(\Delta\eta)^2}\right) \times \underline{C}_A^{i,N\eta,n+1/2} = 2\left(\frac{\nu}{18D_A}\left(N\eta - \frac{1}{2}\right)^2\Delta\eta + \frac{1}{(\Delta\eta)^2}\right) - \left(\frac{4\nu}{27D_A}i\left(N\eta - \frac{1}{2}\right)\Delta\eta\right)\underline{C}_A^{i-2,N\eta,n} + \left(\frac{16\nu}{27D_A}i\left(N\eta - \frac{1}{2}\right)\Delta\eta\right)\underline{C}_A^{i-1,N\eta,n} + \left(2\frac{(i\Delta\xi)^{5/2}}{\Delta\tau} - \frac{4\nu}{9D_A}i\left(N\eta - \frac{1}{2}\right)\Delta\eta\right)\underline{C}_A^{i,N\eta,n} \quad (37)$$

for $j = N\eta$, as $\underline{C}_A^{i,N\eta+1} = 2 - \underline{C}_A^{i,N\eta}$ at the edge of the concentration boundary layer. The sets of finite difference equations for $i = 1, \ldots, N\xi$ exhibit a tridiagonal coefficient matrix and can thus be solved by using the Thomas algorithm [15,16].

For the next half time step, from $\tau_{n+1/2}$ to τ_{n+1}, a second finite difference equivalent to Equation 20 is used, for which the equivalent to $\partial\underline{C}_A/\partial\xi$ is written at the new time level τ_{n+1} and the equivalent to the η-derivatives are written at the old time level $\tau_{n+1/2}$. The resulting equation

$$\left(\frac{4\nu}{27D_A}i\left(j - \frac{1}{2}\right)\Delta\eta\right)\underline{C}_A^{i-2,j,n+1} - \left(\frac{16\nu}{27D_A}i\left(j - \frac{1}{2}\right)\Delta\eta\right)\underline{C}_A^{i-1,j,n+1} + \left(2\frac{(i\Delta\xi)^{5/2}}{\Delta\tau} + \frac{4\nu}{9D_A}i\left(j - \frac{1}{2}\right)\Delta\eta\right)\underline{C}_A^{i,j,n+1} = \left(\frac{1}{(\Delta\eta)^2} - \frac{\nu}{18D_A}\left(j - \frac{1}{2}\right)^2\Delta\eta\right)\underline{C}_A^{i,j-1,n+1/2} + 2\left(\frac{(i\Delta\xi)^{5/2}}{\Delta\tau} - \frac{1}{(\Delta\eta)^2}\right)\underline{C}_A^{i,j,n+1/2} + \left(\frac{1}{(\Delta\eta)^2} + \frac{\nu}{18D_A}\left(j - \frac{1}{2}\right)^2\Delta\eta\right)\underline{C}_A^{i,j+1,n+1/2} \quad (38)$$

is thus implicit in the ξ-direction and explicit in the η-direction. It contains three unknown values of $\underline{C}_A$, arranged along the horizontal part of the T shown in Fig. 4 and three known values of the dependent variable, arranged along the vertical part of that T. Substitution of the boundary conditions at $\xi = 0$ into Equation 38 yields

$$\left(2\frac{(\Delta\xi)^{5/2}}{\Delta\tau} + \frac{16\nu}{27D_A}\left(j - \frac{1}{2}\right)\Delta\eta\right)\underline{C}_A^{1,j,n+1} = \left(\frac{16\nu}{27D_A}\left(j - \frac{1}{2}\right)\Delta\eta\right) + \left(\frac{1}{(\Delta\eta)^2} - \frac{\nu}{18D_A}\left(j - \frac{1}{2}\right)^2\Delta\eta\right)\underline{C}_A^{1,j-1,n+1/2} + 2\left(\frac{(\Delta\xi)^{5/2}}{\Delta\tau} - \frac{1}{(\Delta\eta)^2}\right)\underline{C}_A^{1,j,n+1/2} + \left(\frac{1}{(\Delta\eta)^2} + \frac{\nu}{18D_A}\left(j - \frac{1}{2}\right)^2\Delta\eta\right)\underline{C}_A^{1,j+1,n+1/2} \quad (39)$$

for $i = 1$ and

$$-\left(\frac{32\nu}{27D_A}\left(j - \frac{1}{2}\right)\Delta\eta\right)\underline{C}_A^{1,j,n+1} + \left(2\frac{(2\Delta\xi)^{5/2}}{\Delta\tau} + \frac{8\nu}{9D_A}\left(j - \frac{1}{2}\right)\Delta\eta\right)\underline{C}_A^{2,j,n+1} = -\left(\frac{8\nu}{27D_A}\left(j - \frac{1}{2}\right)\Delta\eta\right) + \left(\frac{1}{(\Delta\eta)^2} - \frac{\nu}{18D_A}\left(j - \frac{1}{2}\right)^2\Delta\eta\right)\underline{C}_A^{2,j-1,n+1/2} + 2\left(\frac{(2\Delta\xi)^{5/2}}{\Delta\tau} - \frac{1}{(\Delta\eta)^2}\right)\underline{C}_A^{2,j,n+1/2} + \left(\frac{1}{(\Delta\eta)^2} + \frac{\nu}{18D_A}\left(j - \frac{1}{2}\right)^2\Delta\eta\right)\underline{C}_A^{2,j+1,n+1/2} \quad (40)$$

for $i = 2$, as $\underline{C}_A^{0,j} = 1$ and $\underline{C}_A^{-1,j} = \underline{C}_A^{1,j}$. The sets of finite difference equations for $j = 1, \ldots, N\eta$ can thus be solved forward from $i = 2$ [15, 17, 18].

The two successive half time steps are to be considered as a single step consisting of two parts, with $\underline{C}_A^{i,j,n+1/2}$ being intermediate values from which the

values of the dependent variable at the new time level are computed. The intermediate values are not representative for the actual values of the dependent variable at $\tau_{n+1/2}$ [16].

The numerical scheme presented has been shown to be stable for any ratio of the time increment to the space increments [15,16].

Electrode current

The electrode current at any instant is given by [2,6]

$$I = -\int_0^R FD_A\left(\frac{\partial C_A}{\partial z}\right)_{z=0}(2\pi r)\mathrm{d}r \qquad (41)$$

and thus by

$$I = -\int_0^1 2\pi R^{3/4} FD_A C_A^{bulk}\left(\frac{135M}{32\nu^3}\right)^{1/4} \times \xi^{-1/4}\left(\frac{\partial \underline{C}_A}{\partial \eta}\right)_{\eta=0}\mathrm{d}\xi \qquad (42)$$

in the computational (ξ, η)-plane. Knowing the time dependent concentration profile of A, the electrode current can be computed from

$$I = -2\pi R^{3/4} FD_A C_A^{bulk}\left(\frac{135M}{32\nu^3}\right)^{1/4} \sum_{i=0}^{N\xi} i^{-1/4} \times \frac{\Delta\xi^{3/4}}{\Delta\eta}(\underline{C}_A^{i,2,n} - \underline{C}_A^{i,1,n}) \qquad (43)$$

4.1.3. Practical computation. Applying the space and equation discretization presented, single step chronoamperometric transients were computed using the Think® Pascal Compiler on a Macintosh II*fx* personal computer.

Convergence was examined by varying the number of grid points and the time increment used. For the geometry of the wall-jet electrode reactor previously reported [1] and volume flow rates ranging from 1.6×10^{-6} to $4.3 \times 10^{-6}\,m^3\,s^{-1}$, a grid of $N\xi = 100 \times N\eta = 50$ points and an initial time increment $\Delta\tau_0 = 5 \times 10^{-8}$, being doubled every ten time steps for the first hundred steps, were found to give convergence to three significant figures in the computed current, using values for ν and D_A typical for aqueous electrolyte solutions ($\nu = 10^{-6}\,m^2\,s^{-1}$; $D_A = 10^{-9}\,m^2\,s^{-1}$). Given the typical values for ν and D_A in aqueous electrolyte solutions and taking into account the theoretical observations made concerning the thickness of the fluid layer adjacent to the impinged surface of a wall-jet electrode reactor, in which the concentration changes occur, the value for $\eta_c \cong 3.96\,(D_A/\nu)^{1/3}$ used in the calculations was chosen to be 0.4. This value for η_c was also used in the calculations of Compton *et al.* [2–5], who examined the influence of the value chosen for η_c on the accuracy of the computed steady state mass transport–limited current and found 0.4 to be optimal. The value for the reactor constant k_r used in the calculations is 0.82 [1].

The calculations require about 2.3 real time seconds per time step. The total number of time steps required to compute a current transient in a time frame of 3 to 5 s, ranges from 200 to 250 depending upon the reactor parameters used.

4.2. *Comparison of computed and experimentally determined current transients*

The validity of the computational method was verified through comparison of calculated with experimentally determined single step chronoamperometric transients, using as a model reaction the reduction of ferricyanide ions at a platinum electrode surface.

Typical examples of the agreement between computed and experimentally determined current–time characteristics are shown in Fig. 5. As can be seen, the computed chronoamperometric transients are in excellent agreement with the experimentally determined ones, over the whole time frame under consideration. In evidence, the computed values of the mass transport–limited current at any instant differ, at the worst, by 3% from the experimentally determined values. Furthermore, it is found that the best fitting between calculated and experimentally determined current transients is obtained using $7.3 \times 10^{-10}\,m^2\,s^{-1}$ as a value for the diffusion coefficient of the ferricyanide ions, which is in accordance with the literature value of $7.7 \pm 0.4 \times 10^{-10}\,m^2\,s^{-1}$ [19, 20].

5. Conclusions

The numerical computational method presented, based on a second order-correct implicit finite difference approach and a space coordinate transformation making the use of a simple Cartesian grid compatible with efficient computing, proved to be an accurate and efficient way of solving problems of mass transport to the impinged surface of a wall-jet electrode reactor. It distinguishes itself in particular by the possibility to perform the calculations on a personal computer.

The computational procedure thus provides the necessary and powerful tool for quantitative electrochemical investigations of the mechanism of electrode processes, using a wall-jet electrode reactor as a hydrodynamic electrode system.

Having the disposal of a suitable wall-jet electrode reactor [1] and the computational method presented to solve the mass transport problems involved, now allows us to achieve further insight in the mechanism of the a.c. electrolytic graining of rolled aluminium substrates, being the main goal of our research.

Acknowledgements

The authors thank M. Raes for the experimental work performed. The financial support of P. Laevers by I.W.T. (Vlaams Instituut voor de Bevordering van het Wetenschappelijk-Technologisch Onderzoek in de Industrie) is gratefully acknowledged.

References

[1] P. Laevers, A. Hubin, H. Terryn and J. Vereecken, *J. Appl. Electrochem.* **25** (1995) 000–000.

[2] R. G. Compton, C. R. Greaves and A. M. Waller, *ibid.* **20** (1990) 575.

[3] A. C. Fisher, R. G. Compton, C. M. A. Brett and A. M. C. F. Oliveira Brett, *J. Electroanal. Chem.* **318** (1991) 53.

[4] C. M. A. Brett, A. M. C. F. Oliveira Brett, A. C. Fisher and R. G. Compton, *ibid.* **334** (1992) 57.

[5] R. G. Compton, A. C. Fisher, M. H. Latham, C. M. A. Brett and A. M. C. F. Oliveira Brett, *J. Appl. Electrochem.* **22** (1992) 1011.

[6] N. Ibl, 'Comprehensive treatise of electrochemistry', vol. 6, (edited by J. O'M Bockris, E. Yeager, B. E. Conway and S. Sarangapani), Plenum Press, New York (1983), p. 1.

[7] C. M. A. Brett and A. M. C. F. Oliveira Brett, 'Comprehensive chemical kinetics', vol. 26, (edited by C. H. Bamford and R. G. Compton), Elsevier, Amsterdam (1986), p. 355.

[8] W. J. Albery and C. M. A. Brett, *J. Electroanal. Chem.* **148** (1983) 201.

[9] *Idem, ibid.* **148** (1983) 211.

[10] H. Schlichting, 'Boundary layer theory', McGraw-Hill, New York (1968).

[11] M. B. Glauert, *J. Fluid Mech.* **1** (1956) 625.

[12] J. Yamada and H. Matsuda, *J. Electroanal. Chem.* **44** (1973) 189.

[13] F. P. Incropera and D. P. De Witt, 'Fundamentals of heat and mass transfer', John Wiley & Sons, New York (1990).

[14] R. G. Compton, A. C. Fisher and G. P. Tyley, *J. Appl. Electrochem.* **21** (1991) 295.

[15] C. Hirsch, 'Numerical computation of internal and external flows', vol. 1, John Wiley & Sons, Chichester (1989).

[16] D. U. von Rosenberg, 'Methods for the Solution of Practical Differential Equations', *in* Modern analytic and computational methods in science and mathematics (edited by R. Bellman), Elsevier, Oxford (1969), p. 87.

[17] B. Van der Linden, 'Elektrochemische Studie van Fotografische Eenheidsprocessen in Gelatinelagen', PhD thesis, Vrije Universiteit Brussel, Brussels (1992).

[18] B. Van der Linden, R. De Keyzer and J. Vereecken, *J. Electroanal. Chem.* **349** (1993) 311.

[19] S. Vandeputte, 'Bijdrage tot het Gebruik van Elektrohydrodynamische Impedantiemetingen voor de Studie van Elektrochemische Systemen', Final Work, Vrije Universiteit Brussel, Brussels (1992).

[20] S. Vandeputte, B. Tribollet, A. Hubin and J. Vereecken, *Electrochim. Acta.* **33**(18) (1994) 2729.